sustainability

MDPI

Article

The Addition of Anthocyanin as a Sensitizer for TiO_2 Nanotubes in a Combined Process of Electrocoagulation and Photocatalysis for Methylene Blue Removal

Indar Kustiningsih [1,*], Hendrini Pujiastuti [1], Denni Kartika Sari [1], Agus Rochmat [1] and Slamet [2]

[1] Department of Chemical Engineering, Universitas Sultan Ageng Tirtayasa, Cilegon 42435, Indonesia; hendrini@untirta.ac.id (H.P.); denni.kartikasari@untirta.ac.id (D.K.S.); agus_rochmat@untirta.ac.id (A.R.)
[2] Department of Chemical Engineering, Universitas Indonesia, Depok 16424, Indonesia; slamet@che.ui.ac.id
* Correspondence: indar.kustiningsih@untirta.ac.id; Tel.: +62-85210723040

Abstract: Photocatalysis with TiO_2 semiconductors is one of several potential methods for removing Methylene Blue (MB) that is environmentally friendly, relatively cheap, and effective. The capability of TiO_2 photocatalysts for degrading MB can be improved by modifying the morphology of TiO_2 into nanotubes and adding anthocyanin sensitizers. The objective of this study was to investigate the effect of anthocyanin sensitizer addition for TiO_2 nanotubes on MB removal using a combined process of electrocoagulation and photocatalysis. TiO_2 nanotubes were prepared through an anodization method with a glycerol electrolyte containing NH_4F of 0.5% w/v and water of 25% v/v. The cathode and anode used in the electrocoagulation process were 316 stainless steel and aluminum, respectively. The characteristics of the resulting TiO_2 nanotubes were analyzed using SEM-EDX, UV–Vis DRS, and XRD analyses. The results showed that the electrocoagulation at a pH of 10 and a voltage of 50 volts resulted in an MB removal efficiency of 57.88%. In the photocatalysis process, sensitizer addition can increase the MB removal efficiency from 19.71% to 29.06%. Furthermore, a combined process of electrocoagulation and photocatalysis without and with sensitizer addition resulted in MB removal efficiencies of 59.66% and 64.30%, respectively.

Keywords: anthocyanin; electrocoagulation; methylene blue; nanotubes; photocatalysis; TiO_2

Citation: Kustiningsih, I.; Pujiastuti, H.; Sari, D.K.; Rochmat, A.; Slamet The Addition of Anthocyanin as a Sensitizer for TiO_2 Nanotubes in a Combined Process of Electrocoagulation and Photocatalysis for Methylene Blue Removal. *Sustainability* **2023**, *15*, 15384. https://doi.org/10.3390/su152115384

Academic Editors: Ying Zhang and Fangke Yu

Received: 13 September 2023
Revised: 18 October 2023
Accepted: 20 October 2023
Published: 27 October 2023

1. Introduction

Waste resulting from textile industries contains dyes with concentrations of 20–30 mg/L, which are hazardous and carcinogenic [1,2]. One of the dyes that are often used in industry is Methylene Blue (MB) ($C_{16}H_{18}N_3SCl$), which is a heterocyclic aromatic molecule [2,3]. The structure formula of MB can be seen in Figure 1. The MB has harmful effects such as vomiting, increased heart rate, cyanosis, digestive system irritation if inhaled, and skin irritation [3,4]. Because of the presence of aromatic amines in the MB structure, the MB is difficult to decompose [3,5].

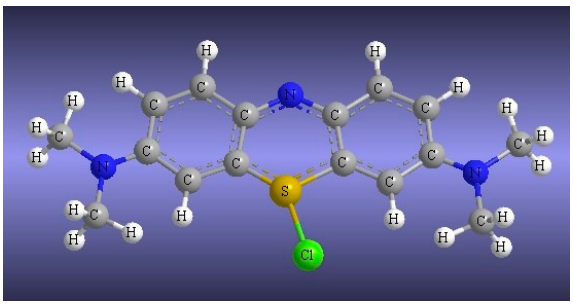

Figure 1. The structure formula of Methylene Blue.

Commonly, MB can be treated through physical and/or chemical treatments, including filtration [6,7], coagulation and precipitation [8,9], adsorption [3,10], ozonation [11], reverse osmosis [12], ion exchange [13], and advanced oxidation [14,15]. However, these treatments need a high operating cost and result in a low pollutant removal efficiency, a high selectivity just for a certain dye group, and harmful intermediate compounds [16].

Photocatalysis is one of the promising methods for removing MB organic dyes in liquid waste because it can degrade MB to CO_2 and H_2O [17–21]. Titanium dioxide (TiO_2) is one of the semiconductors used in photocatalysis. TiO_2 has some advantages, including being stable, non-toxic, corrosion-resistant, abundant in nature, and relatively affordable [18,22,23]. On the other hand, TiO_2 photocatalysts have some disadvantages, including a low specific surface area, a high recombination rate, and a high band gap energy value [24]. The surface of TiO_2 can be improved by modifying its morphology into the shape of nanorods [24,25], nanowires [26,27], and nanotubes [23,26,28,29]. Nanotube morphology is often used because it has a larger surface area and is more effective in photocatalysis than other morphologies [26]. In water treatment, TiO_2 nanotubes can be used in particle or film form (titanium nanotubes arrays (TNTAs)), but the film form (TNTAs) is more attractive because it does not require costly solid–liquid separation [30].

In addition, the effectiveness of TiO_2 photocatalysts can also be improved by the addition of dye-sensitizers. The dye-sensitizer materials function to absorb visible light so electrons can be excited. With the addition of dye-sensitizers, TiO_2 becomes more responsive to visible light. Furthermore, dyes can easily adhere to the catalyst surface; thus, the electrons readily achieve an excited state by photon absorption in the visible light spectrum range [31–33]. Synthetic metal-based dyes can be used as sensitizers, but they can decompose quickly in the working solution [28,29]. Therefore, natural dyes are interesting alternative sensitizers in the photodegradation of aqueous organic contaminants. The natural dyes are harmless, abundant, and inexpensive and contain a hydroxyl carbonyl group to attach to the surface of TiO_2 [34,35]. Anthocyanin, carotenoid, chlorophyll, curcumin, and flavonoid are natural dyes that can be used as sensitizers [31,36–39]. Anthocyanin is a stable sensitizer that can absorb visible light with a high absorption coefficient. Moreover, it can be easily obtained because it is derived from plant sources, such as fruits, blossoms, and vegetables [32,40,41]. Figure 2 shows the structure formula of an anthocyanin molecule attached to TiO_2.

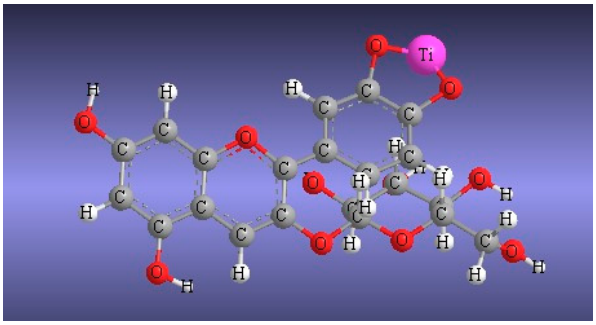

Figure 2. Structure formula of an anthocyanin molecule attached to TiO_2.

Anthocyanin and other natural dyes have been widely used in solar cell applications but are less used in water purification [40,42]. Some studies employed anthocyanins and other natural dyes as sensitizers for TiO_2 nanoparticles; however, there are still very few applications of these sensitizers for TiO_2 nanotubes [32,38,43–46].

To increase pollutant removal efficiency, photocatalysis can be combined with other methods, such as ozone [11,17,47], zeolite [48–50], and electrocoagulation [51–54]. The combination of photocatalysis and electrocoagulation treatments is often conducted in separated reactors [9,55,56], and a small number of researchers employ a single reactor for this purpose. In our previous studies, a combined process of electrocoagulation and photocatalysis in a single reactor for waste treatment was developed [51–53]. However, the

modification of the TiO_2 nanotube arrays (TNTAs) through the sensitizer addition has not been conducted yet.

Based on the information above, the main question addressed by this study is how anthocyanins (as sensitizers) affect the characteristics of the resulting sensitized TNTAs and the performance of the sensitized TNTAs for removing MB through a combined process of electrocoagulation and photocatalysis using a single reactor. Therefore, the goal of this study was to investigate the effect of the addition of anthocyanin sensitizers for TNTAs applied in a combined process of electrocoagulation and photocatalysis, which was operated in a single reactor, for degrading MB. In addition, electrocoagulation alone and photocatalysis alone for degrading MB were also carried out under various operating conditions in this study. The authors hypothesized that the combined process of electrocoagulation and photocatalysis using sensitized TNTAs could result in a higher MB removal efficiency than the electrocoagulation alone, photocatalysis alone, and the combined process using unsensitized TNTAs. This study is original and has not been conducted by other authors yet. The novelty of this study is the utilization of anthocyanins as sensitizers for TNTAs used in a combined process of electrocoagulation and photocatalysis using a single reactor for removing the MB.

2. Materials and Methods

2.1. Material

This study used pro-analytic chemicals, such as ethanol, glycerol, HF, HNO_3, MB, and NH_4F obtained from Sigma-Aldrich (St. Louis, MO, USA). Meanwhile, pure water, aluminum as an anode, and 316 stainless steel as a cathode were collected from local stores.

2.2. Synthesis of TiO_2 Nanotubes (TNTAs)

Titanium plates with dimensions of length, width, and thickness of 8 cm, 4 cm, and 0.5 mm are cleaned using cloth to eliminate adherent dirt. Then, chemical polishing was performed using a mixture of HF (6 mL), HNO_3 (18 mL), and H_2O (36 mL). After that, the plates were cleaned using distilled water, dried at room temperature, and kept in a desiccator. The anodization process was carried out using a two-electrode configuration, in which titanium (Ti) and platinum (Pt) plates were anode and cathode, respectively, with an electrode distance of 1 cm. A DC power supply was utilized as a voltage source. The glycerol electrolyte solution contained NH_4F of 0.5% w/v and water of 25% v/v. Anodization was conducted at a voltage of 50 V for 2 h without heating. After anodizing, the plates were cleaned using distilled water and then dried at room temperature. The calcination process was carried out at 500 °C for 3 h. The scheme of synthesis of TNTAs is shown in Figure 3.

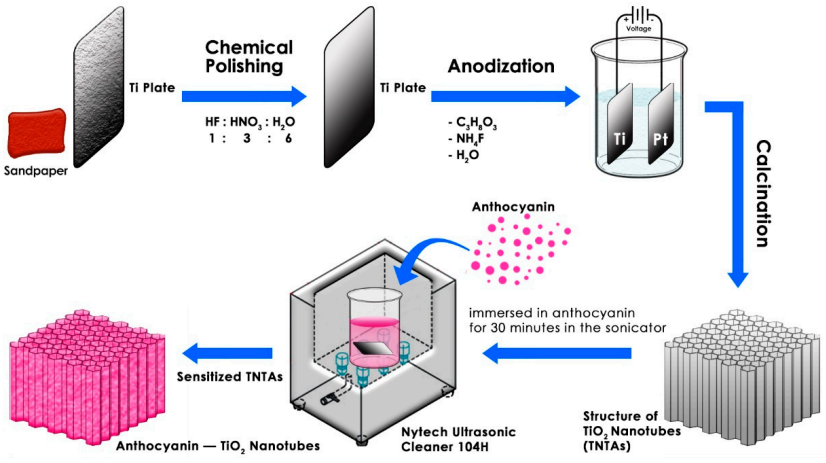

Figure 3. The scheme of synthesis of TNTAs and sensitized TNTAs.

2.3. Preparation of Sensitized TNTAs

Anthocyanin sensitizer was prepared by dissolving synthetic anthocyanin powder in ethanol to generate an anthocyanin solution with concentrations of 40, 80, and 160 ppm. Then, TiO_2 nanotube photocatalysts were immersed in an anthocyanin solution while ultrasonicated for 30 min (see Figure 3). Then, they were dried at room temperature.

2.4. Characterization of Catalyst

Characterization of catalyst was conducted to determine the physical and chemical properties of the resulting photocatalysts. In this study, the catalyst characterization methods included UV–Vis DRS, XRD, SEM-EDX, and FTIR.

2.5. Degradation of Methylene Blue by Electrocoagulation Process

The reactor was filled with 1000 mL of MB solution with a concentration of 10 ppm. A 316 stainless steel plat (length, width, and thickness of 10 cm, 2.5 cm, and 2 mm) as a cathode and two aluminum plates (length, width, and thickness of 10 cm, 2.5 cm, and 2 mm) as anodes were immersed to the solution with an electrode distance of 1 cm. The operating conditions were varied, including voltages (30 V, 40 V, and 50 V) and initial pHs (5, 7, and 10). A DC power supply was used as an electrical current. The electrocoagulation process was carried out for 120 min at room temperature. The liquid samples were taken at minutes 15, 30, 45, 60, 90, and 120. The MB concentrations in the liquid samples were analyzed using UV–Vis spectrophotometry at 663 nm [57].

2.6. Degradation of Methylene Blue by a Combined Process of Photocatalysis and Electrocoagulation

As much as 1000 mL of MB solution with a concentration of 10 ppm was placed in a reactor that was previously filled with sensitized TiO_2 nanotubes. A 316 stainless steel plate (length, width, and thickness of 10 cm, 2.5 cm, and 2 mm) as a cathode and two aluminum plates (length, width, and thickness of 10 cm, 2.5 cm, and 2 mm) as anodes were immersed to the solution with an electrode distance of 1 cm. Afterward, a 120 min irradiation with a 250-watt mercury lamp was conducted. The combined process was carried out for 120 min at room temperature. The liquid samples were taken at minutes 15, 30, 45, 60, 90, and 120. The MB concentrations in the liquid samples were analyzed using UV–Vis spectrophotometry at 663 nm.

2.7. Removal Efficiency of Methylene Blue

The removal efficiency of *MB* was calculated using Equation (1), where C_{MB_i} is the initial *MB* concentration (ppm), and C_{MB_f} is the final *MB* concentration (ppm).

$$MB\ removal\ efficiency = \frac{C_{MB_i} - C_{MB_f}}{C_{MB_i}} \times 100\% \quad (1)$$

3. Results and Discussion

3.1. Effect of Water Content in Glycerol Electrolyte on the Morphology of TiO_2 Nanotube Arrays (TNTAs)

The mechanism of TiO_2 nanotube formation can be explained by Equation (2). Equation (2) describes the anodic oxidation of Ti to generate TiO_2 [58].

$$Ti + 2H_2O \rightarrow TiO_2 + 4H^+ + 4e^- \quad (2)$$

The Ti surface is oxidized to generate a TiO_2 layer, which is then dissolved (electric field-assisted dissolution), producing a tube-like TiO_2 layer. The formation of pores (small pits) is due to dissolving TiO_2 in a solution containing H^+ and F^- ions (resulting from NH_4F), following Equation (3).

$$TiO_2 + 6F^- + 4H^+ \rightarrow (TiF_6)^{2-} + 2H_2O \quad (3)$$

According to Equation (3), Ti and TiO_2 are also chemically dissolved due to the availability of fluoride and the acidic environment. This reaction occurs across the entire porous surface.

Two tests were performed in this investigation, one with a water content of 2% v/v in glycerol, indicating a viscous electrolyte, and one with a water content of 25% v/v in glycerol, representing an aqueous electrolyte. Figure 4 shows the morphology of TNTAs resulting from the anodization process using viscous and aqueous electrolytes. Based on Figure 4, the difference in water content in the electrolyte solution had a significant impact on the morphology of the TNTAs. A higher water content in the electrolyte solution resulted in nanotubes with a larger diameter and a more regular shape. The electrolyte solution with a low water content hindered the mobility of ions in the solution, reducing the TNTA production reaction rate and then producing nanotubes with smaller diameters [58]. Table 1 shows the results of tube diameter measurement.

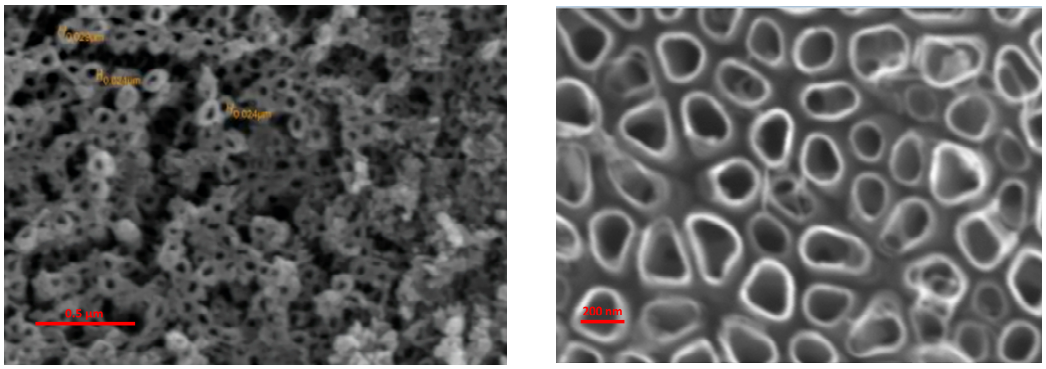

(**a**) (**b**)

Figure 4. SEM results of photocatalyst morphology of TNTAs with water contents in glycerol of (**a**) 2% v/v and (**b**) 25% v/v.

Table 1. Comparison of nanotube diameter size at a variation of water content in glycerol used in the anodization process.

Water Content in Glycerol, *v/v*	Diameter of Tube (nm)
2%	24–29
25%	130–168

The presence of F^- ions can dissolve the resulting oxide layer, and F^- ions were more aggressive in aqueous conditions, resulting in shorter tubes with wider diameters [59]. TiO_2 nanotubes with a mean diameter of 55 nm were produced by anodization at a voltage of 50 volts using an electrolyte solution of ethylene glycol containing 0.5% w/v NH_4F and 2% v/v H_2O [28]. It means that the average diameter of TNTAs generated in this study using glycerol electrolyte solution with a water content of 2% v/v was less than that in the previous study using ethylene glycol electrolyte solution with a water content of 2% v/v [22]. The different values were because ethylene glycol had a lower viscosity (1.612×10^{-2} Pa·s) than glycerol (1.412 Pa·s), so the mobility of ions in the ethylene glycol solution was higher than that in the glycerol solution for the same water content.

3.2. Effect of Water Content in Glycerol Electrolyte on Crystallinity of TNTAs

The goal of calcination is to produce TiO_2 in the anatase crystalline phase. XRD testing was performed to determine the crystallinity of the photocatalysts. Figure 5 shows the XRD test results. Following the XRD result data, anatase crystals were formed either at a water content of 2% v/v or 25% v/v. Peaks of anatase appear at angles of 25.60°, 38.70°, 48.30°, 53.30°, 55.30°, 63.20°, 70.90°, 76.50°, and 82.50° at 2θ position. From Figure 5, it is clear that more frequent and higher peaks are anatase peaks. The peak altitude in the XRD results

reflects the crystallinity level. It means that the higher the anatase peak, the higher the anatase crystal content. The appearance of the anatase peak in Figure 5 indicates that the main component of the catalyst was the anatase crystal. The anatase content in catalysts at a water content of 25% v/v was higher than that at a water content of 2% v/v. Table 2 displays the size of anatase crystals at water contents of 2% v/v and 25% v/v.

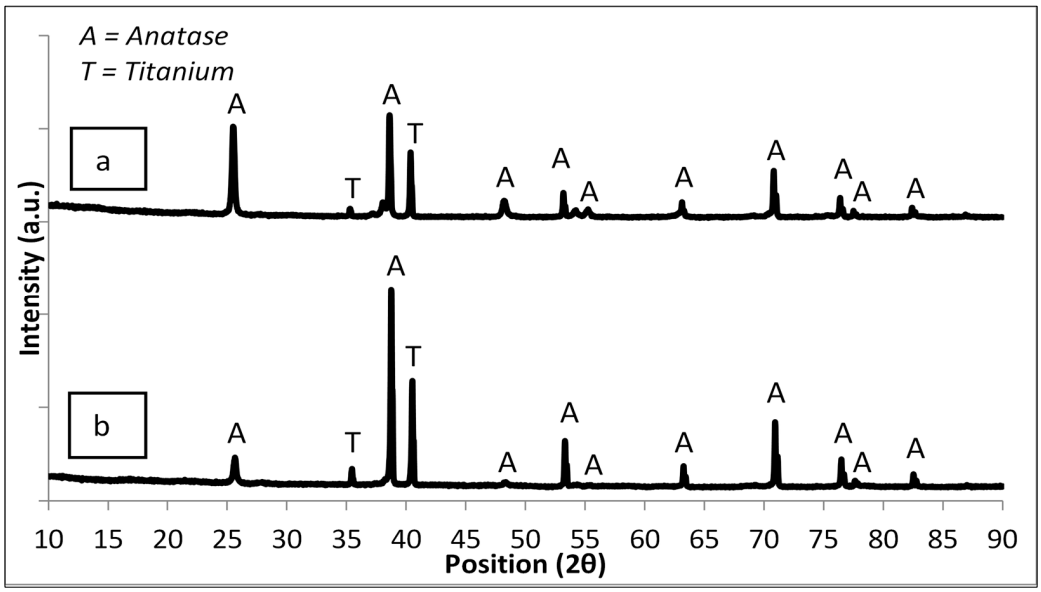

Figure 5. XRD analysis results of catalysts with water contents in glycerol of (**a**) 2% v/v and (**b**) 25% v/v.

Table 2. Comparison of anatase crystal size at a variation of water content in glycerol used in the anodization process.

Water Content in Glycerol, *v/v*	Anatase Crystal Size (nm)
2%	26.6
25%	23.6

The anodization process using glycerol electrolytes with a water content of 2% v/v resulted in anatase crystals with greater crystal sizes than those with a water content of 25% v/v. The resulting anatase crystal size tends to be set at tiny diameters between 10 and 30 nm, and anatase crystals are stabilized in larger-diameter nanotubes [2]. According to the results of catalyst characterization, the water content in the electrolyte solution affected the tube diameter size and the film layer thickness.

Based on the explanation above, the TNTAs resulting from the anodization process using electrolytes with a water content of 25% v/v were better than those with a water content of 2% v/v. Therefore, the electrolyte solution with a water content of 25% v/v was used in the investigation of the effect of sensitizer addition.

3.3. The Effect of Anthocyanin Sensitizer Addition on TNTA Morphology

Ti and O were the primary components of TNTAs, as seen in Figure 6. Other elements, including C, N, and F, were also identified because these elements were absorbed during the anodizing process. After the addition of anthocyanin sensitizer, the C element in TNTAs increased (Figure 6). Based on Figure 6b, TNTAs before sensitization contained Ti, C, and O elements of 67.68, 2.22, and 27.79%wt or 40.55, 5.32, and 49.85% atoms. Then, based on Figure 6d, TNTAs, after sensitization, contained Ti, C, and O elements of 67.96, 4.51, and 25.37%wt or 40.63, 10.74, and 45.39% atoms. This demonstrated that the increase in C element was caused by the diffusion of anthocyanins into TNTAs during the immersion-

ultrasonication process. Zyoud et al. also reported that the C element in the catalyst increased after the addition of anthocyanin sensitizers [31].

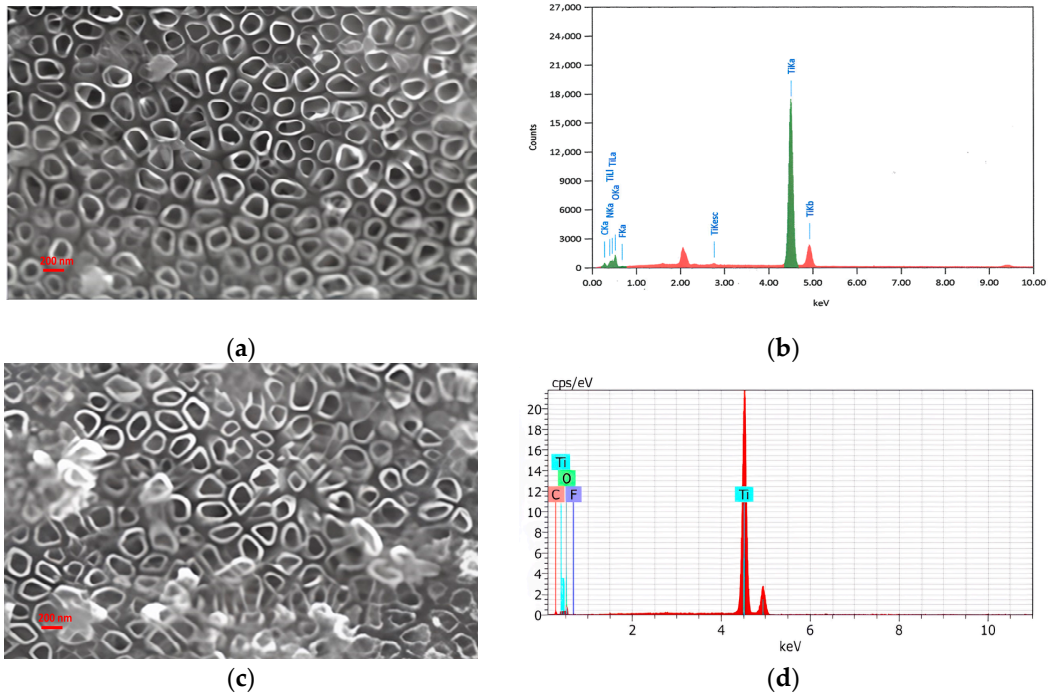

Figure 6. (**a**) SEM for TNTAs before sensitization, (**b**) EDX for TNTAs before sensitization, (**c**) SEM for TNTAs after sensitization, (**d**) EDX for TNTAs after sensitization. Electrolyte solution with a water content of 25% v/v and anthocyanin sensitizer addition of 160 ppm.

3.4. The Effect of Anthocyanin Sensitizer Addition on Crystallinity

The effect of adding anthocyanin sensitizers on the crystallinity of TNTAs was examined using XRD. The results of the XRD analysis are shown in Figure 7. For TNTAs without sensitizers, peaks at 2 θ at angles of 35.40° and 40.50° indicate diffraction from titanium (Ti). Meanwhile, peaks at 2 θ at angles of 25.60°, 38.70°, 48.30°, 53.30°, 55.30°, 63.20°, 70.90°, 76.50°, and 82.50° indicate diffraction from anatase. In detail, sensitized TNTAs had higher anatase peaks than unsensitized TNTAs, especially at an angle of 38.70°. This means that the sensitizer addition successfully increased the anatase crystal content in TNTAs.

The anatase phase crystal sizes without and with sensitizer additions are shown in Table 3. The addition of anthocyanin sensitizers caused the anatase phase crystal size to expand because there was an increase in temperature throughout the process of sensitizing TNTA catalysts with an anthocyanin sensitizer with ultrasound for 30 min. Following the addition of the sensitizer, the calcination effect caused the anatase crystal size of the catalyst to become larger.

3.5. The Effect of Anthocyanin Addition on the Band Gap Energy of TNTAs

The effect of anthocyanin addition on the band gap energy was examined using a UV–Vis DRS. Figure 8a,b depict the results of UV–Vis DRS analysis. Figure 8 depicts the results of UV–Vis DRS investigations to calculate the band gap energy using a Tauc plot, as well as extrapolating Tauc graphics on the linear part of the graph and cutting the x-axis. Figure 8 shows that unmodified TNTAs had a band gap energy of 3.25 eV, which was consistent with reports in the literature and confirmed that TiO_2 was only active when exposed to UV light [31,60]. The band gap energy for TNTAs + anthocyanin was reduced to 2.5 eV. When a photon is absorbed by the anthocyanin molecule, an electron is excited from its highest occupied molecular orbital (HOMO) to its lowest unoccupied molecular

orbital (LUMO). Subsequently, a state of relaxation is achieved as a result of the process of electron loss to the conduction band (CB) of TNTAs [43,44,61].

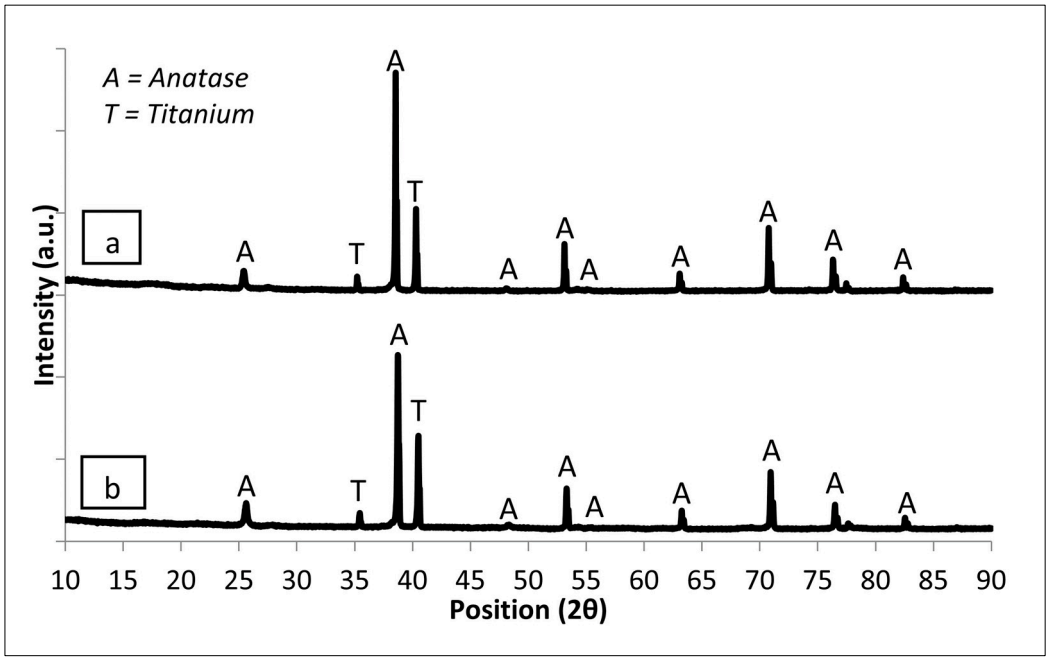

Figure 7. Results of XRD analysis of catalysts (**a**) with sensitizer addition and (**b**) without sensitizer addition. Electrolyte solution with a water content of 25% v/v and anthocyanin sensitizer addition of 160 ppm.

Table 3. Comparison of anatase crystal size as a result of the addition of anthocyanin sensitizer.

Catalyst	Anatase Crystal Size (nm)
TNTAs	23.6
TNTAs + anthocyanin 160 ppm	28.7

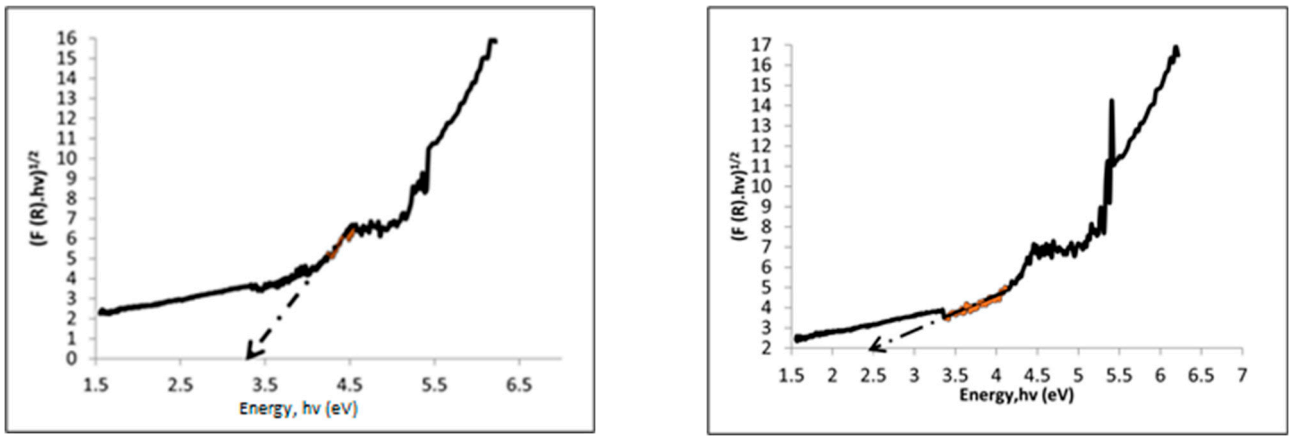

(**a**) (**b**)

Figure 8. Tauc plot of Kubelka–Munk function transformation vs. band gap energy (eV) for (**a**) TNTAs and (**b**) for TNTAs + anthocyanin. Electrolyte solution with a water content of 25% v/v and anthocyanin addition of 160 ppm.

The UV–Vis DRS spectra in Figure 9 exhibited an increase in absorbance values in the wavelength range of 380–800 nm due to the addition of 160 ppm anthocyanin sensitizer.

This shows that catalysts with sensitizers can absorb photons more efficiently in the visible light spectrum.

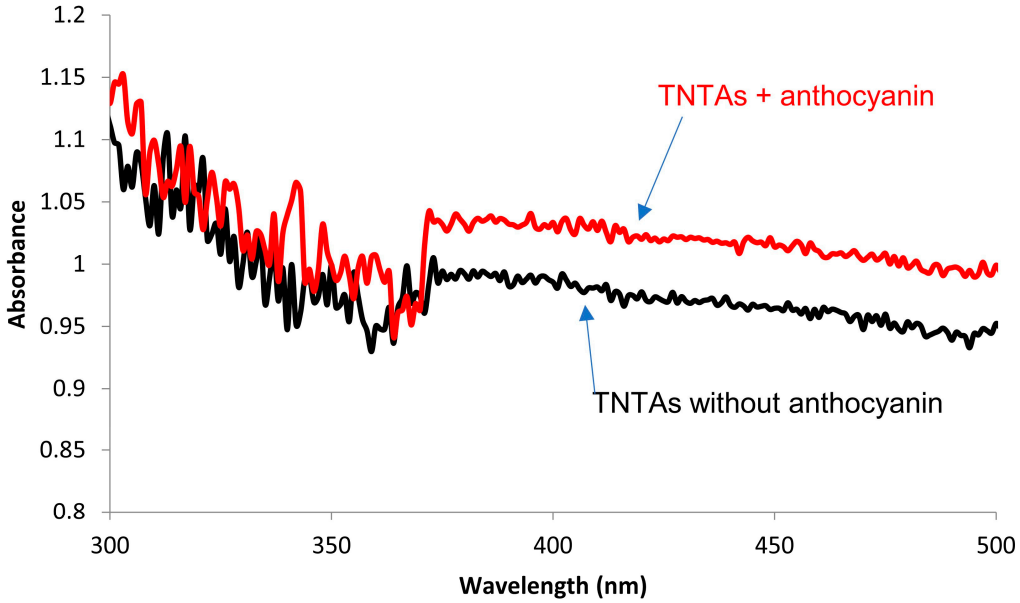

Figure 9. UV–Vis DRS spectra of catalysts with and without anthocyanin addition. Electrolyte solution with a water content of 25% v/v and anthocyanin sensitizer addition of 160 ppm.

3.6. Photocatalytic Process for Methylene Blue (MB) Degradation

3.6.1. The Effect of Initial pH

Figure 10 demonstrates that the rate of MB photodegradation increases when the initial pH increases from 5 to 10. After 120 min, initial pHs of 5, 7, and 10 resulted in MB removal efficiencies of 15.38, 17.47, and 19.71%, respectively. Hence, MB degradation was best achieved at an initial pH of 10, resulting in the highest MB removal efficiency. This was because the initial pH of 10 changed the charge on the surface of the TNTA photocatalysts to be negatively charged, so MB (which was a cationic dye) became more easily adsorbed, thereby increasing the photodegradation rate of MB. The adsorption rate of MB on the catalyst surface affected the variance in reaction rate.

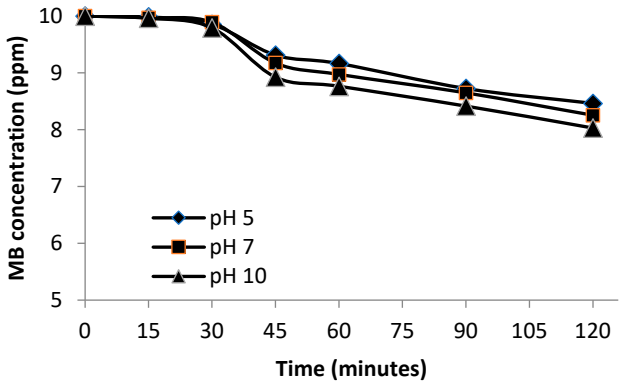

Figure 10. Effect of initial pH variation on the performance of TNTA photocatalyst for degrading MB. Electrolyte solution with a water content of 25% v/v in the anodization process and anthocyanin sensitizer addition of 160 ppm.

The findings of this study were consistent with the findings of a previous study by Dariani et al., who reported that an increase in initial pH from 3 to 11 can improve the MB removal efficiency through a photocatalysis process using 0.5 g of TiO_2 with a particle size of 200 nm and a process time of 5 h [62]. At high pH levels, the catalyst surfaces were

dominated by negative charges, and there was a significant interaction between the catalyst surfaces and the dye cations, resulting in strong adsorption. On the other hand, at low pH, the catalytic surfaces and coloring molecules were positively charged. The surface of TiO_2 had a neutral charge at a pH of 6.8. In an acidic medium (pH < 6.8), the surface of TiO_2 had a positive charge; in a base medium (pH > 6.8), it had a negative charge [62].

3.6.2. The Effect of Sensitizer Addition for TNTAs on Photocatalytic Performance

The decrease in MB concentration during the photocatalysis process at various sensitizer additions is shown in Figure 11. An increase in sensitizer addition from 0 to 160 ppm successfully increased the rate of MB degradation. After 120 min, MB removal efficiencies at sensitizer additions of 0 (without sensitizer addition), 40, 80, and 160 ppm were 19.71, 19.94, 24.65, and 29.06%, respectively. The presence of sensitizers reduced the band gap energy, making the catalyst more receptive to photons and increasing the number of excited electrons. The addition of anthocyanin sensitizers did not affect the shape of the catalyst's nanotubes, so the area of the catalytic surface remained vast. The XRD data revealed that the addition of sensitizers increased the anatase crystal size. Anthocyanins had a hydroxyl (OH) group, so the anthocyanin-sensitized catalyst surface became hydrophilic. As a consequence, MB molecules were closer to the catalyst surface, and the tension between the catalyst surfaces and the MB solution became lower.

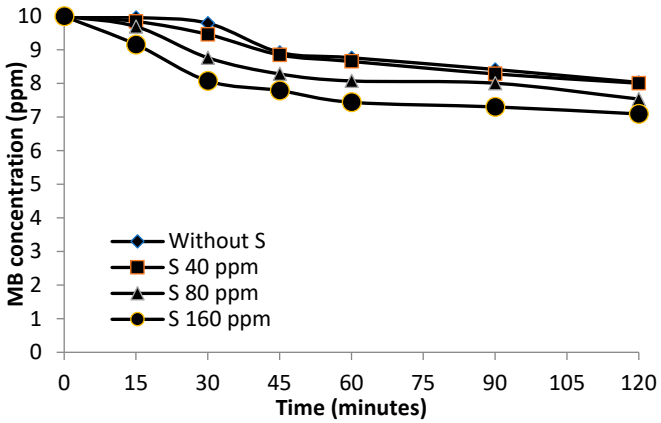

Figure 11. Effect of addition of anthocyanin sensitizers on the performance of TNTA photocatalysts for degrading MB. Electrolyte solution with a water content of 25% v/v in the anodization process and initial pH of photocatalysis process of 10.

The MB removal efficiency in the case without sensitizer addition was 19.71%. Furthermore, after the sensitizer addition of 40 ppm, the MB removal efficiency increased to 19.94%. It shows that the sensitizer addition of 40 ppm to TNTAs had no significant effect on the MB removal efficiency. However, the sensitizer addition of 160 ppm significantly increased the MB removal efficiency value, namely 29.06%.

According to Angulo et al., dye molecules can easily attach to the catalyst surface and acquire an excited state via photon absorption in the visible light spectrum region [33]. The injection of electrons from anthocyanin dye molecules into the conduction bands of TNTA photocatalysts increased the quantities of reactive oxygen species (ROS) and accelerated the breakdown of MB. Anthocyanin sensitizers absorbed visible light and allowed electrons to be activated. TNTA photocatalysts became more responsive to visible light when anthocyanin sensitizers were added [31,33]. Figure 12 depicts a scheme of MB photodegradation by TNTAs with anthocyanin sensitizers.

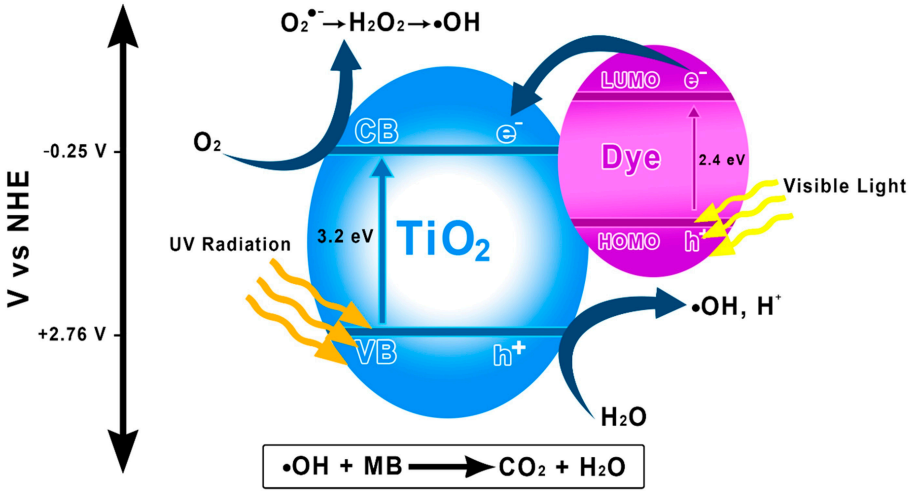

Figure 12. The scheme of MB photodegradation by TNTAs with anthocyanin sensitizers.

3.7. Electrocoagulation Process for Methylene Blue (MB) Degradation

3.7.1. Effect of Voltage

The effect of voltage on the electrocoagulation process for degrading MB is shown in Figure 13. Based on Figure 13, the higher the voltage was applied, the faster the MB degradation rate would be. After 120 min, the electrocoagulation process at voltages of 30, 40, and 50 volts resulted in MB removal efficiencies of 29.91, 43.35, and 51.85%, respectively. An increase in voltage was directly proportional to an increase in electrical current (I). The larger the electrical current was applied, the more the ions were generated at the anode and cathode, resulting in enhanced coagulant formation in the solution [63]. The more the coagulants were generated in the solution, the more the MB molecules could be adsorbed, enhancing the MB removal efficiency.

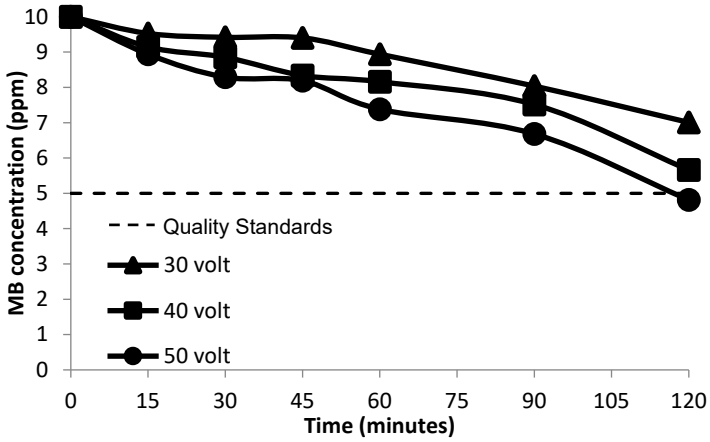

Figure 13. The profiles of MB concentrations during the electrocoagulation process at various voltages.

The waste quality standard (MB of 5 ppm) was reached in around 120 min at a voltage of 50 volts. The linear equations in Figure 14 can be used to approximate the reduction of the MB compound as a function of time during the electrocoagulation process. Through these linear equations, the waste quality standard for MB can be achieved after being processed through an electrocoagulation process at voltages of 30, 40, and 50 volts for 215 min, 153 min, and 120 min, respectively. Furthermore, the relationship between voltage and time needed to reach the waste quality standard can be predicted through the linear equations shown in Figure 15. Through the equations in Figures 14 and 15, the electrocoagulation process time required to reach the MB effluent quality standard at various voltages can be estimated within a voltage range of 30–50 V.

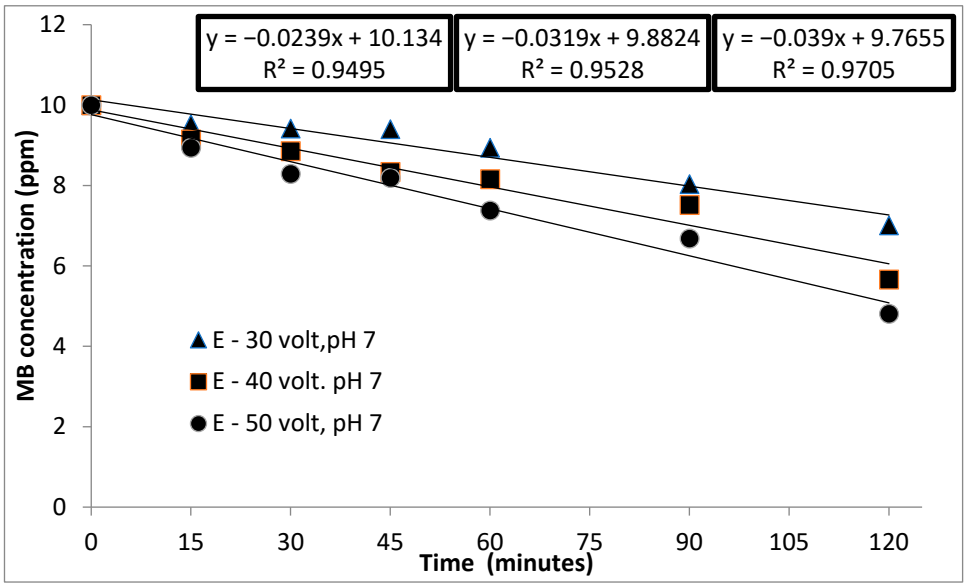

Figure 14. The relationship between MB concentration and electrocoagulation process time.

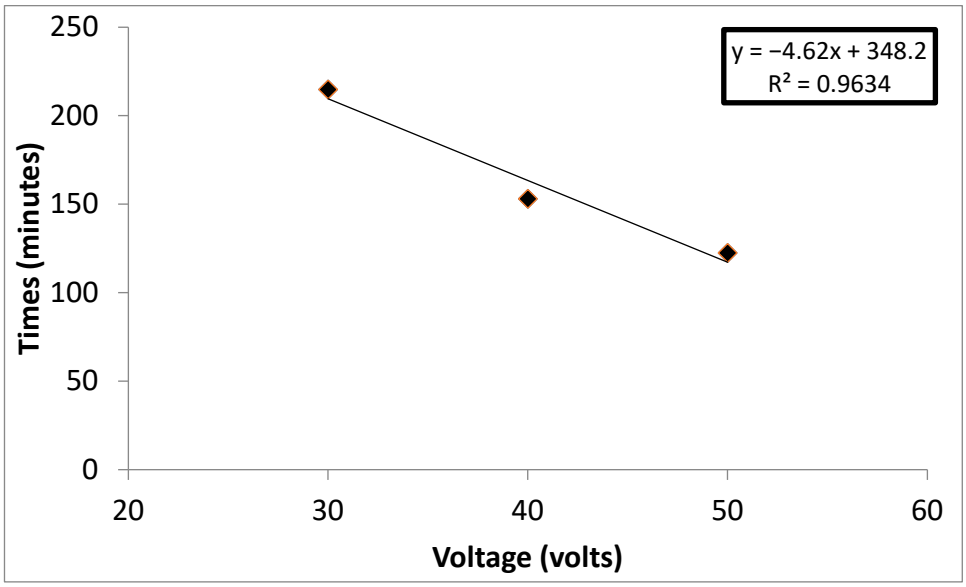

Figure 15. The relationship between voltage and time to achieve waste quality standards.

The degradation of MB during electrocoagulation can be modeled through the first-order kinetic model, following Equation (4).

$$-\frac{dC}{dt} = kC \tag{4}$$

The first-order kinetic model can be rearranged by integration to become Equations (5) and (6) with the boundary conditions of $C = C_0$ at $t = 0$ and $C = C_t$ at $t = t$

$$In\left(\frac{C_t}{C_0}\right) = -kt \tag{5}$$

$$lnC_t = -kt + lnC_0 \tag{6}$$

Equation (5) can be arranged into Equation (6).

$$C_t = C_0 \exp(-kt) \tag{7}$$

where C_t is the concentration of MB at t time (ppm), C_0 is the initial concentration of MB (ppm), t is the electrocoagulation time (minutes), and k is the reaction rate constant (min^{-1}). The kinetic constants (k) can be obtained through optimization with the objective function of the Sum of Squared Error (SSE) using Microsoft Excel. The formula of SSE is shown in Equation (7).

$$SSE = \sum_{i=1}^{n} \left(C_{t\,model_i} - C_{t\,experiment_i} \right)^2 \tag{8}$$

where $C_{t\,model}$ is the concentration of MB at time t (ppm) obtained from modeling, and $C_{experiment}$ is the concentration of MB at time t (ppm) obtained from the experiment. The first-order kinetic model was successfully used to simulate the MB concentration profiles during the electrocoagulation process with SSE values of 0.522–0.725. Plotting between experimental data and modeled data is shown in Figure 16. Then, the reaction rate constants at 30, 40, and 50 V were 0.0025, 0.0040, and 0.0053 min^{-1}, respectively.

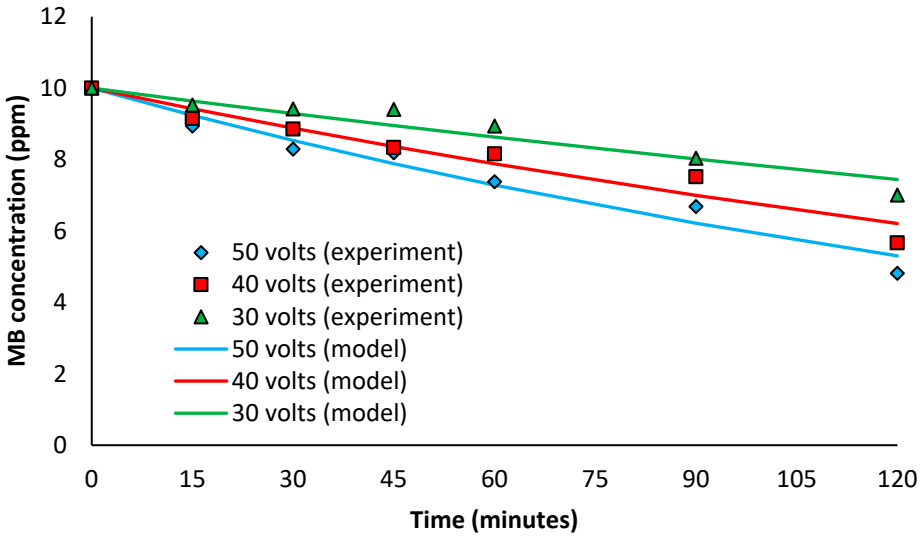

Figure 16. Plotting between experimental data and modeled data obtained from the first-order kinetic model.

3.7.2. The Effect of pH

In this stage, the electrocoagulation process was carried out at a voltage of 50 volts with a variation of initial pH of 5, 7, and 10. Figure 17 shows the profiles of MB concentration during the electrocoagulation process at various initial pHs. The electrocoagulation at initial pHs of 5, 7, and 10 resulted in MB removal efficiencies of 39.49, 51.85, and 57.88%, respectively. Hence, an increase in initial pH from 5 to 10 increased MB removal efficiency values. The highest MB removal efficiency of 57.88% was obtained at an initial pH of 10. According to Figure 17, after 2 h, the electrocoagulation process at initial pHs of 7 and 10 can decrease MB concentrations to meet the waste quality standard for MB. Meanwhile, the time to reach the waste quality standard at pH 5 can be predicted through linear regression of the relationship between MB concentration and time. As a result, for initial pHs of 5, 7, and 10, the time required to achieve the waste quality criteria was 147, 115, and 75 min, respectively. It can be concluded that an initial pH of 10 can lower the MB concentration to the quality standards in less time than initial pHs of 5 and 7. During electrocoagulation, Al^{3+} ions are generated at the anode, and OH^- ions are generated at the cathode. The Al^{3+} can react with OH^- to form various Al species. At high pH, the dominant Al species

is $Al(OH)_3$, while at low pH, the dominant Al species is Al^{3+} ions. Hence, the $Al(OH)_3$ coagulant amount is higher at an initial pH of 10 than at initial pHs of 5 and 7. The $Al(OH)_3$ coagulants can adsorb MB. Thus, the MB was easier to remove at initial pH of 10 than at initial pHs of 5 and 7. As a consequence, the initial pH needed a shorter time to decrease the MB concentration from 10 ppm to 5 ppm (quality standard). In line with this study, Muttaqin et al. reported that an initial pH of 10 resulted in a higher $Al(OH)_3$ amount than initial pHs of 5 and 7, so an initial pH of 10 resulted in a higher MB removal efficiency than initial pHs of 5 and 7 [64].

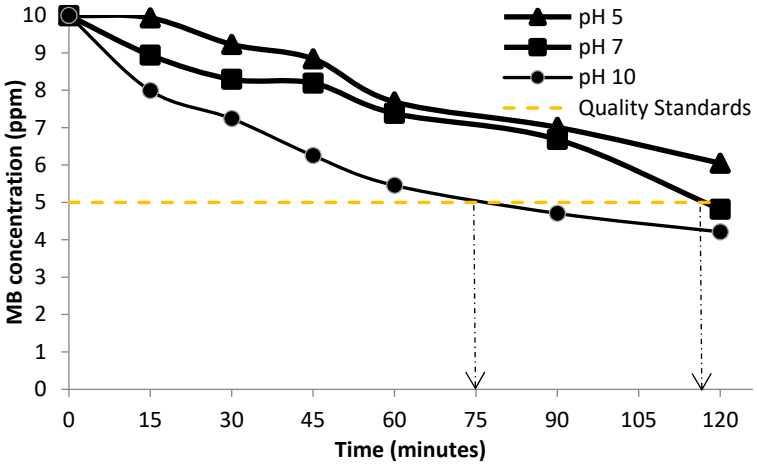

Figure 17. The profiles of MB concentrations during the electrocoagulation process at various initial pHs. Voltage of 50 Volts.

The rate of MB decolorization and the amount of sludge were affected by the initial pHs. As shown in Table 4, an increase in initial pH increased the sludge amount and the decolorization rate. At higher pH levels, $Al(OH)_3$ coagulations were generated in large amounts. The more the amount of $Al(OH)_3$ was generated in the solution, the higher the dye decolorization efficiency was obtained [42]. The solution pH has a significant impact on the electrocoagulation process performance [8].

Table 4. Sludge weights in the electrocoagulation process at various initial pHs.

Initial pH of Electrocoagulation	Sludge Weight (g)
5	2.42
7	2.83
10	3.85

3.8. A Combined Process of Electrocoagulation and Photocatalysis for Methylene Blue (MB) Degradation

At this stage, a combined process of electrocoagulation–photocatalysis without and with anthocyanin sensitizer addition for degrading MB compounds was performed. The profiles of MB concentrations during photocatalysis (P), electrocoagulation (E), and the combination process of E-P are shown in Figure 18. After 120 min, the electrocoagulation process achieved an MB removal efficiency of 57.88%, while the combined process of electrocoagulation and photocatalysis without sensitizer addition achieved a higher MB reduction efficiency of 59.66%. The presence of anthocyanin sensitizers in the combined process of electrocoagulation and photocatalysis can improve the MB removal efficiency from 59.66% to 64.30%. In this condition, waste quality standards can be reached within 48 min, whereas combining electrocoagulation and photocatalysis without a sensitizer takes 60 min (Figure 18). The presence of photocatalysis could assist in the degradation of MB dyes into non-hazardous compounds for the environment.

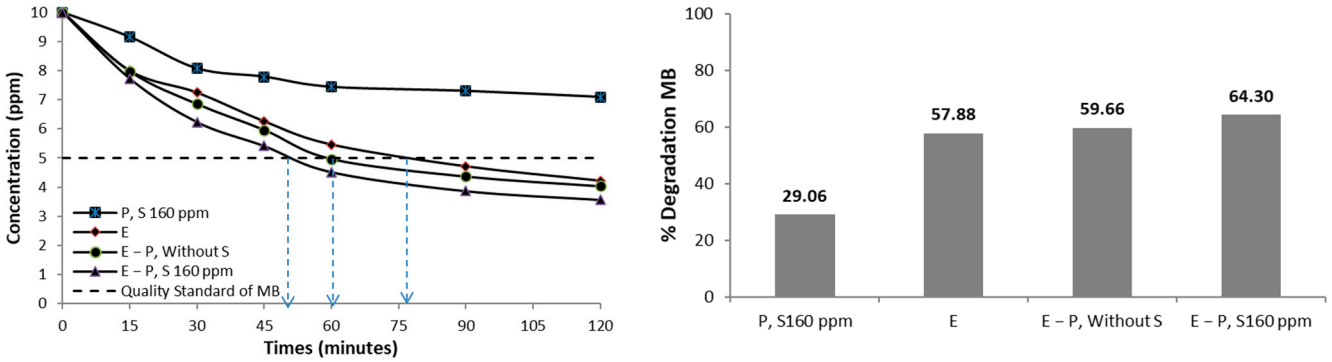

(**a**) (**b**)

Figure 18. (**a**) Profiles of MB concentrations during the electrocoagulation, photocatalysis, and combined process of electrocoagulation and photocatalysis; (**b**) the total MB removal efficiencies after 120 min. Electrolyte solution with a water content of 25% v/v in the anodization process, anthocyanin sensitizer addition of 160 ppm, initial pH of 10, and voltage of 50 Volts. E = electrocoagulation, P = photocatalysis, E−P = combined process of electrocoagulation and photocatalysis. Blue arrows in (**a**) show the times that are needed by the processes to decrease the MB concentration from 10 ppm to 5 ppm (quality standard).

This was also reflected in the sludge's color of the combined process without sensitizer addition, which was more faded when compared to the sludge's color of the combined process without sensitizer addition. In other words, the presence of anthocyanin sensitizers in the combined process can improve its ability to degrade MB. The addition of anthocyanin sensitizers can improve photon absorption in the visible light spectrum, allowing TNTA photocatalysts to degrade MB dyes more effectively. The addition of sensitizers reduced the band gap energy, making the catalyst more receptive to photons and increasing the number of excited electrons. The addition of anthocyanin sensitizers did not change the morphology of the catalyst nanotubes, so the area of the catalytic surface remained vast.

The combined process of electrocoagulation and photocatalysis can decrease MB concentrations to waste quality standards in less time than the electrocoagulation alone and the photocatalysis alone. Figure 18 shows that the electrocoagulation alone needed around 75 min to reach waste quality criteria, while the combined process of electrocoagulation and photocatalysis with sensitizer addition needed only 48 min to reach waste quality criteria.

Table 5 provides a comparison of the results of this study with those of other studies. According to Table 5, the combined process in this study resulted in a higher MB removal per catalyst than that in a previous study [51] because this study used anthocyanin sensitizers, while a previous study did not use sensitizers [51]. However, another previous study [61] resulted in a higher MB removal per catalyst than this study, where the previous study [61] utilized the photocatalysis process with anthocyanin sensitizers, while this study utilized the combined process anthocyanin sensitizers. It was due to the difference in the ratio of MB/catalyst, namely 0.3125 mg/cm^2 in this study and 0.125 mg/cm^2 in the previous study [61]. Furthermore, the other previous studies (see Table 5) reported different pollutant removal efficiencies because of the differences in the types of methods, types and forms of photocatalysts, types of sensitizers, and types of pollutants.

Table 5. Comparison of the results of the current research with those from previous studies.

No	Methods	Photocatalyst	Power/Film	Sensitizer	Pollutant	Experiment	Results	References
1	E-P with a single reactor	TiO_2 nanotubes array	Film	Anthocyanin	Methylene Blue (MB)	Volume of 1000 mL, MB of 10 ppm, ratio of MB/catalyst of 0.3125 mg/cm^2	The removal efficiency of MB was 64.5%. The MB removal per catalyst was 2.016%/cm^2.	This study
2	E-P with a single reactor	Fe-TiO_2 nanotubes arrays	Film	-	Methylene Blue–ciprofloxacin (MB-CIP)	Volume of 1000 mL, 10 ppm MB-10 ppm CIP, film surface of 64 cm^2, ratio of MB/catalyst of 0.1562 mg/cm^2, ratio of CIP/catalyst of 0.1562 mg/cm^2	The removal efficiencies of CIP and MB were 90% and 100%, respectively. The CIP removal per catalyst was 1.406%/cm^2. The MB removal per catalyst was 1.5625%/cm^2.	[51]
3	E-P with separated reactors	Ag-TiO_2 P25	Powder	-	Tartrazine (TTZ)	Volume of 3 L, TTZ of 50 mg/L, 100 mg/L Ag-TiO_2 P25, ratio of TTZ/catalyst of 0.5 mg/mg	The mineralization of TTZ was 74%. The TTZ removal per catalyst was 0.2467%/mg.	[56]
4	E-P with separated reactor	Immobilized ZnO	Film	-	Petroleum	Initial COD of 1000 mg/L, ratio of petroleum/catalyst of 0.2711 mg/mg	The removal efficiency of COD was 94% after 60 min. The petroleum removal per catalyst was 0.0255%/mg	[9]
5	E-P with separated reactors	TiO_2 and ZnO	Powder	-	Olive washing wastewater	Initial pH of 6.9, voltage of 12.5 V, ZnO of 1 g/L	The removal efficiencies of COD and color were 88% and 100%, respectively.	[55]
6	E-P with a single reactor	ZnO	Powder	-	Malathion	Initial malathion concentration of 45 mg/L, ZNO of 1.6 mg/L, volume of 500 mL, ratio of malathion/catalyst of 28.125 mg/mg	The removal efficiency of malathion was 68.33%. The malathion removal per catalyst was 85.41%/mg.	[54]

Table 5. *Cont.*

No	Methods	Photocatalyst	Power/Film	Sensitizer	Pollutant	Experiment	Results	References
7	P	TiO_2 nanoparti-cles	Powder	Anthocyanin	Methylene Blue (MB)	Anthocyanin from blackberry, hibiscus, Urucum, Curcuma	The decolorization efficiency was 51–73%.	[45]
8	P	TiO_2 P25	Thin Film	Anthocyanin	Methylene Blue (MB)	Volume of 25 mL, MB of 10 ppm, surface area of 2 cm^2, ratio of MB/catalyst of 0.125 mg/cm^2	The decolorization efficiency was 25.6%. The MB removal per catalyst was 12.8%/cm^2.	[61]
9	P	TiO_2 nanoparti-cles	Powder	Chlorophyll	Methylene Blue (MB)	Volume of 100 mL, MB of 20 ppm, catalyst of 1 g/L, ratio of MB/catalyst of 20 mg/mg	The removal efficiency of MB was 85%. The MB removal per catalyst was 8.5%/mg.	[65]
10	P	TiO_2 aerogel	Powder	Anthocyanin	Cr (VI)	Volume of 50 mL, Cr(VI) concentration of 15 ppm, ratio of Cr(VI)/catalyst of 0.75 mg/mg	The removal efficiency of Cr(VI) was 100%. The Cr(VI) removal per catalyst was 2%/mg.	[46]

3.9. The Color and Weight of Sludges Resulting from the Electrocoagulation Process and the Combined Process of Electrocoagulation and Photocatalysis

The sludges from the electrocoagulation process and the combined process were analyzed. The sludge from the electrocoagulation process without MB was used as a control. Then, the control sludge was compared to the sludges from the electrocoagulation process, the combined process with and without sensitizer additions. Figure 19 shows the sludges of the electrocoagulation process and the combined processes.

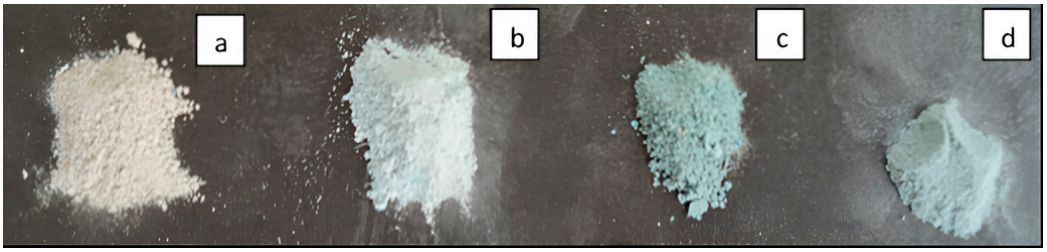

Figure 19. The result of sludges in the process of electrocoagulation and electrocoagulation–photocatalysis combination. (**a**) blank; (**b**) electrocoagulation; (**c**) combined process without sensitizer; (**d**) combined process with sensitizer.

Based on Figure 19, there was a difference in the color of sludges resulting from the electrocoagulation process and the combined process. The electrocoagulation process has three steps, namely electrolysis, coagulation, and flotation [42,66]. During this process, Al is oxidized to Al^{3+} at the anode, while water is reduced to H^+ and OH^- ions at the cathode. Then, Al^{3+} reacts with OH ions to form coagulants of $Al(OH)_3$, which can adsorb contaminants, while H_2 is produced through water electrolysis. The H_2 gas aids in the

removal of contaminants through flotation [55,67,68]. Detailed reactions occurring during the electrocoagulation process are as follows:

$$\text{At Anode} : Al_{(s)} \rightarrow Al^{3+}_{(aq)} + 3e^{-} \quad (9)$$

$$\text{At Cathode} : 2H_2O_{(aq)} + 2e^{-} \rightarrow 2OH^{-}_{(aq)} + H_{2(g)} \quad (10)$$

$$\text{Chemical Reaction} : Al^{3+}_{(aq)} + 3OH^{-}_{(aq)} \rightarrow Al(OH)_{3(s)} \quad (11)$$

$$\text{Total Reaction} : 2Al_{(s)} + 6H_2O_{(aq)} \rightarrow 2Al(OH)_{3(s)} + 3H_{2(g)} \quad (12)$$

Equation (11) is applicable for alkaline medium [64]. Then, $Al(OH)_3$ can adsorb MB to form sludge (MB-$Al(OH)_3$), as shown in Equation (12).

$$Al(OH)_{3(s)} + MB \rightarrow (MB - Al(OH)_3)_{(s)} \quad (13)$$

Light and catalysts are required for the photocatalysis process to accelerate chemical reactions. When subjected to UV light with an energy larger than the band gap energy, these semiconductor materials create electron pairs $\left(e^{-}_{cb}\right)$ and holes, which can reduce and oxidize compounds. The reactions that occur in the photocatalytic process for waste degradation are as follows:

$$TiO_2 + hv \rightarrow TiO_2(h^{+} + e^{-}_{cb}) \quad (14)$$

$$TiO_2(h^{+}) + H_2O \rightarrow \ OH\bullet + H^{+} \quad (15)$$

$$TiO_2\left(e^{-}_{cb}\right) + O_2 \rightarrow O^{-}_{2}\bullet \quad (16)$$

$$OH\bullet \text{ or } O^{-}_{2}\bullet + \ MB \rightarrow CO_2 + H_2 \quad (17)$$

Therefore, the electrocoagulation process involves the adsorption of MB dye, but the combined process involves the degradation of MB dye by TNTA photocatalysts as well as the adsorption process. The MB removal mechanisms during a combined process of electrocoagulation and photocatalysis are shown in Figure 20 in detail.

The sludge formed from the electrocoagulation process was not blue compared to the sludge formed from the combined process of electrocoagulation–photocatalysis. Methylene Blue (MB) can turn into colorless leuco-Methylene Blue (LMB) due to a hydrogenation reaction, while the LMB can turn into MB due to an oxidation reaction [68]. A hydrogenation reaction is a reaction between hydrogen and another compound. During electrocoagulation, hydrogen is generated at the cathode. The presence of hydrogen might cause MB to change to LMB. Then, the coagulants might adsorb the LMB, thereby resulting in colorless sludge.

Meanwhile, during the combined process, the hydrogen resulted from the electrocoagulation, while the oxygen resulted from the photocatalysis process. The presence of hydrogen would change MB to LMB, and then the presence of oxygen would change LMB to MB again. Furthermore, the coagulants adsorbed MB, thereby resulting in blue sludge.

The sludges resulting from the combined process without and with sensitizers also appear to differ in color. When compared to the sludge from the electrocoagulation process without sensitizers, the sludge from the combined process with the sensitizers has a more fading color. The combined process with sensitizers degraded more MB than the combined process without sensitizers. As a consequence, the coagulants in the combined process with sensitizers adsorbed less MB than those in the combined process without sensitizers. Therefore, the sludge from the combined process with sensitizers has a more fading color.

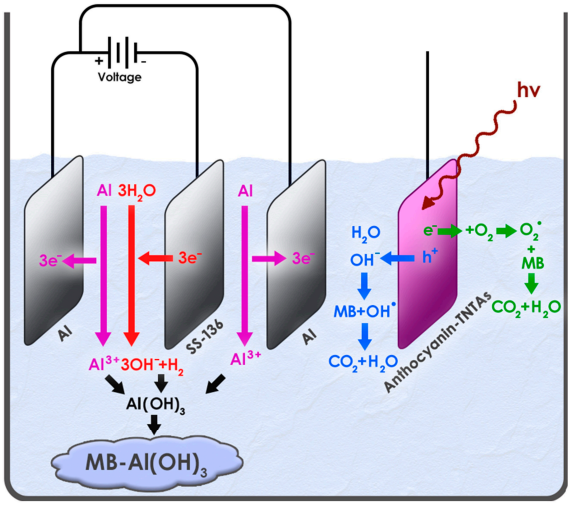

Figure 20. The MB removal mechanisms during a combined process of electrocoagulation and photocatalysis.

Table 6 shows the weight of the sludge produced in the electrocoagulation process and the combined process without and with sensitizer addition, indicating that there is a difference in the weight of the sludge produced. The sludge produced in the combined process was less than the sludge produced in the electrocoagulation alone. This was because, in the combined process, some OH^- ions became OH• radicals due to the photocatalysis process, so only a small amount of OH^- ions reacted with Al^{3+} ions to form $Al(OH)_3$ coagulants.

Table 6. Sludge weight in the electrocoagulation process and the combined process of electrocoagulation–photocatalysis.

Method	Sludge Weight (g)
Electrocoagulation	3.85
Combination without Sensitizer	2.15
Combination with Sensitizer	1.6

4. Conclusions

The water content in the glycerol electrolyte solution used in the anodization process significantly affected the diameter of nanotubes and the size of TNTAs. Specifically, a higher water content led to a bigger diameter while simultaneously causing a decrease in crystal size. The incorporation of anthocyanins into TNTAs did not alter the structural characteristics of the nanotubes. However, it led to an increase in the crystal size of the anatase phase from 23.6 nm to 28.7 nm and a decrease in the band gap energy from 3.2 eV to 2.5 eV. Utilization of the sensitized TNTAs in the combined process of electrocoagulation and photocatalysis can increase the removal efficiency from 59.66% to 64.30%. The results of this study confirmed the authors' hypothesis that the combined process of electrocoagulation and photocatalysis using sensitized TiO_2 nanotube photocatalysts can result in a higher MB removal efficiency than the electrocoagulation alone, photocatalysis alone, and the combined process using unsensitized TiO_2 nanotube photocatalysts. In general, the total cost of the photocatalysis process using sensitized TiO_2 nanotubes is higher than the total cost of the photocatalysis process using unsensitized TiO_2 nanotubes because there is the cost of synthesis of sensitized TiO_2 nanotubes in the former. Then, the MB removal efficiency in the former does not exceed 65%. Therefore, a feasibility study of the process is necessary to be conducted in the future.

This study has some limitations. This study used a wavelength of 663 nm to measure the MB concentration during electrocoagulation and photocatalysis at various pH conditions. However, in theory, the optimum wavelength of MB may be affected by pH

levels. For the next study, this needs to be noted. Furthermore, the composition of sludges resulting from electrocoagulation, photocatalysis, and the combined process was not analyzed. Thus, this needs to be noted in the next study. The future research prospect might be the application of the combined process with sensitized TiO_2 nanotube photocatalysts for treating Rhodamine B, methyl orange, as well as real organic wastes. In addition, the economic analysis and feasibility study of the combined process are necessary to be conducted in the future. This study did not analyze the stability and recyclability of the sensitized TiO_2 nanotubes. Therefore, these analyses need to be carried out in the next research. Also, this study did not analyze the intermediate products resulting from the combined process. Hence, identification and characterization of these intermediates need to be conducted in the future to know detailed mechanisms during the combined process.

Author Contributions: Conceptualization, I.K., S. and A.R.; methodology, I.K. and A.R.; software, H.P. and I.K.; validation, S.; formal analysis, H.P. and D.K.S.; investigation, H.P. and D.K.S.; resources H.P. and I.K.; data curation, H.P., I.K. and S.; writing—original draft preparation, H.P. and I.K.; writing—review and editing, S.; visualization, I.K.; supervision, I.K. and S.; project administration, D.K.S.; funding acquisition, I.K. All authors have read and agreed to the published version of the manuscript.

Funding: This research was funded by the Directorate General of Higher Education, Ministry of National Education Indonesia, through HIBAH FUNDAMENTAL 2023, grant number B/609/UN43.9/PT.00.03.

Informed Consent Statement: Not applicable.

Data Availability Statement: Data will be made available on request.

Acknowledgments: The main financial support from the Directorate General of Higher Education, Ministry of National Education Indonesia, through HIBAH FUNDAMENTAL 2023, is gratefully acknowledged.

Conflicts of Interest: The authors declare no conflict of interest.

References

1. Karim, A.V.; Shriwastav, A. Degradation of Ciprofloxacin Using Photo, Sono, and Sonophotocatalytic Oxidation with Visible Light and Low-Frequency Ultrasound: Degradation Kinetics and Pathways. *Chem. Eng. J.* **2020**, *392*, 124853. [CrossRef]
2. Vasiraja, N.; Saravana Sathiya Prabhahar, R.; Joshua, A. Preparation and Physio–Chemical Characterisation of Activated Carbon Derived from Prosopis Juliflora Stem for the Removal of Methylene Blue Dye and Heavy Metal Containing Textile Industry Effluent. *J. Clean. Prod.* **2023**, *397*, 136579. [CrossRef]
3. Marahel, F.; Mombeni Goodajdar, B.; Niknam, L.; Faridnia, M.; Pournamdari, E.; Mohammad Doost, S. Ultrasonic Assisted Adsorption of Methylene Blue Dye and Neural Network Model for Adsorption of Methylene Blue Dye by Synthesised Mn-Doped PbS Nanoparticles. *Int. J. Environ. Anal. Chem.* **2023**, *103*, 3059–3080. [CrossRef]
4. Mustafa, F.H.A.; Gad ElRab, E.K.M.; Kamel, R.M.; Elshaarawy, R.F.M. Cost-Effective Removal of Toxic Methylene Blue Dye from Textile Effluents by New Integrated Crosslinked Chitosan/Aspartic Acid Hydrogels. *Int. J. Biol. Macromol.* **2023**, *248*, 125986. [CrossRef]
5. Zhao, Q.; Zhang, L.; Wang, X.; Jia, X.; Xu, P.; Zhao, M.; Dai, R. Simultaneous Efficient Adsorption and Photocatalytic Degradation of Methylene Blue over Iron(III)-Based Metal–Organic Frameworks: A Comparative Study. *Transit. Met. Chem.* **2019**, *44*, 789–797. [CrossRef]
6. Li, Q.; Li, Y.; Ma, X.; Du, Q.; Sui, K.; Wang, D.; Wang, C.; Li, H.; Xia, Y. Filtration and Adsorption Properties of Porous Calcium Alginate Membrane for Methylene Blue Removal from Water. *Chem. Eng. J.* **2017**, *316*, 623–630. [CrossRef]
7. Pasichnyk, M.; Gaálová, J.; Minarik, P.; Václavíková, M.; Melnyk, I. Development of Polyester Filters with Polymer Nanocomposite Active Layer for Effective Dye Filtration. *Sci. Rep.* **2022**, *12*, 973. [CrossRef]
8. Ihaddaden, S.; Aberkane, D.; Boukerroui, A.; Robert, D. Removal of Methylene Blue (Basic Dye) by Coagulation-Flocculation with Biomaterials (Bentonite and Opuntia Ficus Indica). *J. Water Process Eng.* **2022**, *49*, 102952. [CrossRef]
9. Keramati, M.; Ayati, B. Petroleum Wastewater Treatment Using a Combination of Electrocoagulation and Photocatalytic Process with Immobilized ZnO Nanoparticles on Concrete Surface. *Process Saf. Environ. Prot.* **2019**, *126*, 356–365. [CrossRef]
10. Meili, L.; Lins, P.V.S.; Costa, M.T.; Almeida, R.L.; Abud, A.K.S.; Soletti, J.I.; Dotto, G.L.; Tanabe, E.H.; Sellaoui, L.; Carvalho, S.H.V.; et al. Adsorption of Methylene Blue on Agroindustrial Wastes: Experimental Investigation and Phenomenological Modelling. *Prog. Biophys. Mol. Biol.* **2019**, *141*, 60–71. [CrossRef]
11. Babar, M.; Munir, H.M.S.; Nawaz, A.; Ramzan, N.; Azhar, U.; Sagir, M.; Tahir, M.S.; Ikhlaq, A.; Mohammad Azmin, S.N.h.; Mubashir, M.; et al. Comparative Study of Ozonation and Ozonation Catalyzed by Fe-Loaded Biochar as Catalyst to Remove Methylene Blue from Aqueous Solution. *Chemosphere* **2022**, *307*, 135738. [CrossRef] [PubMed]

12. Li, H.; Lin, Y.; Luo, Y.; Yu, P.; Hou, L. Relating Organic Fouling of Reverse Osmosis Membranes to Adsorption during the Reclamation of Secondary Effluents Containing Methylene Blue and Rhodamine B. *J. Hazard. Mater.* **2011**, *192*, 490–499. [CrossRef] [PubMed]
13. El-Moselhy, M.M.; Kamal, S.M. Selective Removal and Preconcentration of Methylene Blue from Polluted Water Using Cation Exchange Polymeric Material. *Groundw. Sustain. Dev.* **2018**, *6*, 6–13. [CrossRef]
14. Kumar, M.S.; Sonawane, S.H.; Pandit, A.B. Degradation of Methylene Blue Dye in Aqueous Solution Using Hydrodynamic Cavitation Based Hybrid Advanced Oxidation Processes. *Chem. Eng. Process. Process Intensif.* **2017**, *122*, 288–295. [CrossRef]
15. Mohammed, H.A.; Khaleefa, S.A.; Basheer, M.I. Photolysis of methylene blue dye using an advanced oxidation process (ultraviolet light and hydrogen peroxide). *J. Eng. Sustain. Dev.* **2022**, *25*, 59–67. [CrossRef]
16. Huseynov, K.; Ramazanov, M.; Garib, M. Photocatalytic degradation of organic pollutants in air by application of titanium dioxide nanoparticles. *Chem. Eng. Trans.* **2017**, *60*, 241–246. [CrossRef]
17. Sonmez, B.; Baser, E.; Gel, O.Y. Photodecolourization of Methylene Blue by Fe- and Cd-Incorporated Titania-Supported Zeolite Clinoptilolite. *Microporous Mesoporous Mater.* **2022**, *340*, 112001. [CrossRef]
18. Xing, Z.; Zhang, J.; Cui, J.; Yin, J.; Zhao, T.; Kuang, J.; Xiu, Z.; Wan, N.; Zhou, W. Recent Advances in Floating TiO_2-Based Photocatalysts for Environmental Application. *Appl. Catal. B Environ.* **2018**, *225*, 452–467. [CrossRef]
19. Tan, H.; Zhang, Y.; Li, B.; Yang, H.; Hou, H.; Huang, Q. Preparation of TiO_2-Coated Glass Flat Membrane and Its Photocatalytic Degradation of Methylene Blue. *Ceram. Int.* **2023**, *49*, 17236–17244. [CrossRef]
20. Yang, R.; Zhu, Z.; Hu, C.; Zhong, S.; Zhang, L.; Liu, B.; Wang, W. One-Step Preparation (3D/2D/2D) BiVO4/FeVO4@rGO Heterojunction Composite Photocatalyst for the Removal of Tetracycline and Hexavalent Chromium Ions in Water. *Chem. Eng. J.* **2020**, *390*, 124522. [CrossRef]
21. Yang, R.; Zhong, S.; Zhang, L.; Liu, B. PW12/CN@Bi_2WO_6 Composite Photocatalyst Prepared Based on Organic-Inorganic Hybrid System for Removing Pollutants in Water. *Sep. Purif. Technol.* **2020**, *235*, 116270. [CrossRef]
22. Abdullah, H.; Khan, M.M.R.; Ong, H.R.; Yaakob, Z. Modified TiO_2 Photocatalyst for CO_2 Photocatalytic Reduction: An Overview. *J. CO_2 Util.* **2017**, *22*, 15–32. [CrossRef]
23. Roy, P.; Berger, S.; Schmuki, P. TiO_2 Nanotubes: Synthesis and Applications. *Angew. Chem. Int. Ed.* **2011**, *50*, 2904–2939. [CrossRef] [PubMed]
24. Singh, J.; Juneja, S.; Soni, R.K.; Bhattacharya, J. Sunlight Mediated Enhanced Photocatalytic Activity of TiO_2 Nanoparticles Functionalized CuO-Cu_2O Nanorods for Removal of Methylene Blue and Oxytetracycline Hydrochloride. *J. Colloid Interface Sci.* **2021**, *590*, 60–71. [CrossRef] [PubMed]
25. You, M.; Kim, T.G.; Sung, Y.-M. Synthesis of Cu-Doped TiO_2 Nanorods with Various Aspect Ratios and Dopant Concentrations. *Cryst. Growth Des.* **2010**, *10*, 983–987. [CrossRef]
26. Khan, M.A.M.; Ansari, A.A.; Choudhary, P.; Ahmed, J.; Kumar, S.; Hussain, S. Reduced Graphene Oxide Supported Ag-Loaded Brookite TiO2 Nanowires: Enhanced Photocatalytic Degradation Performance and Electrochemical Energy Storage Applications. *Diam. Relat. Mater.* **2023**, *139*, 110397. [CrossRef]
27. Safajou, H.; Khojasteh, H.; Salavati-Niasari, M.; Mortazavi-Derazkola, S. Enhanced Photocatalytic Degradation of Dyes over Graphene/Pd/TiO_2 Nanocomposites: TiO_2 Nanowires versus TiO_2 Nanoparticles. *J. Colloid Interface Sci.* **2017**, *498*, 423–432. [CrossRef]
28. Abdullah, M.; Kamarudin, S.K. Titanium Dioxide Nanotubes (TNT) in Energy and Environmental Applications: An Overview. *Renew. Sustain. Energy Rev.* **2017**, *76*, 212–225. [CrossRef]
29. Wtulich, M.; Szkoda, M.; Gajowiec, G.; Jurak, K.; Trykowski, G.; Lisowska-Oleksiak, A. Hydrothermal Modification of TiO_2 Nanotubes in Water and Alkali Metal Electrolytes ($LiNO_3$, $NaNO_3$, KNO_3) — Direct Evidence for Photocatalytic Activity Enhancement. *Electrochim. Acta* **2022**, *426*, 140802. [CrossRef]
30. Feng, Y.; Rijnaarts, H.H.M.; Yntema, D.; Gong, Z.; Dionysiou, D.D.; Cao, Z.; Miao, S.; Chen, Y.; Ye, Y.; Wang, Y. Applications of Anodized TiO_2 Nanotube Arrays on the Removal of Aqueous Contaminants of Emerging Concern: A Review. *Water Res.* **2020**, *186*, 116327. [CrossRef]
31. Zyoud, A.H.; Saleh, F.; Helal, M.H.; Shawahna, R.; Hilal, H.S. Anthocyanin-Sensitized TiO_2 Nanoparticles for Phenazopyridine Photodegradation under Solar Simulated Light. *J. Nanomater.* **2018**, *2018*, 2789616. [CrossRef]
32. Diaz-Uribe, C.; Vallejo, W.; Camargo, G.; Muñoz-Acevedo, A.; Quiñones, C.; Schott, E.; Zarate, X. Potential Use of an Anthocyanin-Rich Extract from Berries of Vaccinium Meridionale Swartz as Sensitizer for TiO_2 Thin Films—An Experimental and Theoretical Study. *J. Photochem. Photobiol. A Chem.* **2019**, *384*, 112050. [CrossRef]
33. Diaz-Angulo, J.; Lara-Ramos, J.; Mueses, M.; Hernández-Ramírez, A.; Li Puma, G.; Machuca-Martínez, F. Enhancement of the Oxidative Removal of Diclofenac and of the TiO_2 Rate of Photon Absorption in Dye-Sensitized Solar Pilot Scale CPC Photocatalytic Reactors. *Chem. Eng. J.* **2020**, *381*, 122520. [CrossRef]
34. Khalil, M.; Gunlazuardi, J.; Ivandini, T.A.; Umar, A. Photocatalytic Conversion of CO_2 Using Earth-Abundant Catalysts: A Review on Mechanism and Catalytic Performance. *Renew. Sustain. Energy Rev.* **2019**, *113*, 109246. [CrossRef]
35. Rekha, M.; Kowsalya, M.; Ananth, S.; Vivek, P.; Jauhar, R.O.M.U. Current–Voltage Characteristics of New Organic Natural Dye Extracted from Terminalia Chebula for Dye-Sensitized Solar Cell Applications. *J. Opt.* **2019**, *48*, 104–112. [CrossRef]
36. Pujiastuti, H.; Kustiningsih, I.; Slamet, S. Improvement of the Efficiency of TiO_2 Photocatalysts with Natural Dye Sensitizers Anthocyanin for the Degradation of Methylene Blue. *J. Rekayasa Kim. Lingkung.* **2021**, *16*, 84–99. [CrossRef]

37. Degradation of Ciprofloxacin Antibiotic Waste Using TiO2 Nanotube with Addition of Anthocyanin Dye-Sensitizer in Photocatalysis Process: Review | Fidarohman | Jurnal Rekayasa Kimia & Lingkungan. Available online: https://jurnal.usk.ac.id/RKL/article/view/28520 (accessed on 5 October 2023).
38. Díaz-Uribe, C.; Vallejo, W.; Campos, K.; Solano, W.; Andrade, J.; Muñoz-Acevedo, A.; Schott, E.; Zarate, X. Improvement of the Photocatalytic Activity of TiO_2 Using Colombian Caribbean Species (Syzygium Cumini) as Natural Sensitizers: Experimental and Theoretical Studies. *Dyes Pigments* **2018**, *150*, 370–376. [CrossRef]
39. Chandel, M.; Thakur, M.; Sharma, A.; Pathania, D.; Kumar, A.; Singh, L. Chlorophyll Sensitized $(BiO)_2CO_3/CdWO_4$/rGO Nano-Hybrid Assembly for Solar Assisted Photo-Degradation of Chlorzoxazone. *Chemosphere* **2022**, *305*, 135472. [CrossRef]
40. Elseman, A.M. *Solar Cells: Theory, Materials and Recent Advances*; BoD—Books on Demand: Norderstedt, Germany, 2021; ISBN 978-1-83881-016-0.
41. Mohammed, H.A.; Khan, R.A. Anthocyanins: Traditional Uses, Structural and Functional Variations, Approaches to Increase Yields and Products' Quality, Hepatoprotection, Liver Longevity, and Commercial Products. *Int. J. Mol. Sci.* **2022**, *23*, 2149. [CrossRef]
42. Daneshvar, N.; Ashassi Sorkhabi, H.; Kasiri, M.B. Decolorization of Dye Solution Containing Acid Red 14 by Electrocoagulation with a Comparative Investigation of Different Electrode Connections. *J. Hazard. Mater.* **2004**, *112*, 55–62. [CrossRef]
43. Giang, N.T.H.; Thinh, N.T.; Hai, N.D.; Loc, P.T.; Thu, T.N.A.; Loan, N.H.P.; Quang, D.M.; Anh, L.D.; Truong An, V.N.T.; Phong, M.T.; et al. Application of TiO_2 Nanoparticles with Natural Chlorophyll as the Catalyst for Visible Light Photocatalytic Degradation of Methyl Orange and Antibacterial. *Inorg. Chem. Commun.* **2023**, *150*, 110513. [CrossRef]
44. Zyoud, A.; Hilal, H. Investigation of Curcumin as Sensitizer for Anatase TiO_2 Nanoparticles in Photodegradation of of Phenazopyridine with Visible Light. *PhytoChem BioSub J.* **2014**, *8*, 127–137.
45. Goulart, S.; Jaramillo Nieves, L.J.; Dal Bó, A.G.; Bernardin, A.M. Sensitization of TiO_2 Nanoparticles with Natural Dyes Extracts for Photocatalytic Activity under Visible Light. *Dyes Pigments* **2020**, *182*, 108654. [CrossRef]
46. Yang, H.; Jiang, L.; Li, Y.; Li, G.; Yang, Y.; He, J.; Wang, J.; Yan, Z. Highly Efficient Red Cabbage Anthocyanin Inserted TiO_2 Aerogel Nanocomposites for Photocatalytic Reduction of Cr(VI) under Visible Light. *Nanomaterials* **2018**, *8*, 937. [CrossRef]
47. Mecha, A.C.; Chollom, M.N. Photocatalytic Ozonation of Wastewater: A Review. *Environ. Chem. Lett.* **2020**, *18*, 1491–1507. [CrossRef]
48. Mahamud, M.; Taddesse, A.M.; Bogale, Y.; Bezu, Z. Zeolite Supported $CdS/TiO_2/CeO_2$ Composite: Synthesis, Characterization and Photocatalytic Activity for Methylene Blue Dye Degradation. *Mater. Res. Bull.* **2023**, *161*, 112176. [CrossRef]
49. Gong, P.; Li, B.; Kong, X.; Shakeel, M.; Liu, J.; Zuo, S. Hybriding Hierarchical Zeolite with Pt Nanoparticles and Graphene: Ternary Nanocomposites for Efficient Visible-Light Photocatalytic Degradation of Methylene Blue. *Microporous Mesoporous Mater.* **2018**, *260*, 180–189. [CrossRef]
50. Girma, S.; Taddesse, A.M.; Bogale, Y.; Bezu, Z. Zeolite-Supported g-C3N4/ZnO/CeO_2 Nanocomposite: Synthesis, Characterization and Photocatalytic Activity Study for Methylene Blue Dye Degradation. *J. Photochem. Photobiol. A Chem.* **2023**, *444*, 114963. [CrossRef]
51. Muttaqin, R.; Pratiwi, R.; Ratnawati; Dewi, E.L.; Ibadurrohman, M.; Slamet. Degradation of Methylene Blue-Ciprofloxacin and Hydrogen Production Simultaneously Using Combination of Electrocoagulation and Photocatalytic Process with Fe-TiNTAs. *Int. J. Hydrogen Energy* **2022**, *47*, 18272–18284. [CrossRef]
52. Slamet, S.; Kurniawan, R. Degradation of Tartrazine and Hydrogen Production Simultaneously with Combination of Photocatalysis-Electrocoagulation. *AIP Conf. Proc.* **2018**, *2024*, 020064. [CrossRef]
53. Slamet, N.S.; Shobri, A.; Anindria, F.A.; Mauricio, R.; Tafsili, M.A.B.; Slamet, S. Treatment of Batik Industry Waste with a Combination of Electrocoagulation and Photocatalysis. *Chem. Eng.* **2018**, *9*, 936–943. [CrossRef]
54. Rangel-Peraza, J.G.; Prado, M.A.R.; Amabilis-Sosa, L.E.; Bustos-Terrones, Y.A.; Ramírez-Pereda, B. Malathion Removal through Peroxi-Electrocoagulation and Photocatalytic Treatments. Optimization by Statistical Analysis. *Int. J. Electrochem. Sci.* **2020**, *15*, 8253–8264. [CrossRef]
55. Ates, H.; Dizge, N.; Yatmaz, H.C. Combined Process of Electrocoagulation and Photocatalytic Degradation for the Treatment of Olive Washing Wastewater. *Water Sci. Technol.* **2016**, *75*, 141–154. [CrossRef] [PubMed]
56. Santos, L.M.; Amorim, K.P.D.; Andrade, L.S.; Batista, P.S.; Trovó, A.G.; Machado, A.E.H. Dye Degradation Enhanced by Coupling Electrochemical Process and Heterogeneous Photocatalysis. *J. Braz. Chem. Soc.* **2015**, *26*, 1817–1823. [CrossRef]
57. Blanckenberg, A.; Malgas-Enus, R. Raspberry-like Gold-Decorated Silica (SSx–AMPS–Au) Nanoparticles for the Reductive Discoloration of Dyes. *SN Appl. Sci.* **2019**, 787. [CrossRef]
58. Ratnawati; Gunlazuardi, J.; Slamet. Development of Titania Nanotube Arrays: The Roles of Water Content and Annealing Atmosphere. *Mater. Chem. Phys.* **2015**, *160*, 111–118. [CrossRef]
59. Regonini, D.; Bowen, C.R.; Jaroenworaluck, A.; Stevens, R. A Review of Growth Mechanism, Structure and Crystallinity of Anodized TiO_2 Nanotubes. *Mater. Sci. Eng. R Rep.* **2013**, *74*, 377–406. [CrossRef]
60. Madhusudan Reddy, K.; Manorama, S.V.; Ramachandra Reddy, A. Bandgap Studies on Anatase Titanium Dioxide Nanoparticles. *Mater. Chem. Phys.* **2003**, *78*, 239–245. [CrossRef]
61. Diaz-Uribe, C.; Vallejo, W.; Romero, E.; Villareal, M.; Padilla, M.; Hazbun, N.; Muñoz-Acevedo, A.; Schott, E.; Zarate, X. TiO_2 Thin Films Sensitization with Natural Dyes Extracted from Bactris Guineensis for Photocatalytic Applications: Experimental and DFT Study. *J. Saudi Chem. Soc.* **2020**, *24*, 407–416. [CrossRef]

62. Dariani, R.S.; Esmaeili, A.; Mortezaali, A.; Dehghanpour, S. Photocatalytic Reaction and Degradation of Methylene Blue on TiO_2 Nano-Sized Particles. *Optik* **2016**, *127*, 7143–7154. [CrossRef]
63. Liu, C.; Neale, Z.G.; Cao, G. Understanding Electrochemical Potentials of Cathode Materials in Rechargeable Batteries. *Mater. Today* **2016**, *19*, 109–123. [CrossRef]
64. Muttaqin, R.; Ratnawati, R.; Slamet, S. Batch Electrocoagulation System Using Aluminum and Stainless Steel 316 Plates for Hospital Wastewater Treatment. *IOP Conf. Ser. Earth Environ. Sci.* **2022**, *963*, 012056. [CrossRef]
65. Krishnan, S.; Shriwastav, A. Application of TiO_2 Nanoparticles Sensitized with Natural Chlorophyll Pigments as Catalyst for Visible Light Photocatalytic Degradation of Methylene Blue. *J. Environ. Chem. Eng.* **2021**, *9*, 104699. [CrossRef]
66. Liu, N.; Wu, Y. Removal of Methylene Blue by Electrocoagulation: A Study of the Effect of Operational Parameters and Mechanism. *Ionics* **2019**, *25*, 3953–3960. [CrossRef]
67. Holt, P.; Barton, G.; Mitchell, C. Electrocoagulation as a Wastewater Treatment. In Proceedings of the Third Annual Australian Environmental Engineering Research Event, Castlemaine, VIC, Australia, 23–26 November 1999.
68. Jegadeesan, C.; Somanathan, A.; Jeyakumar, R.B.; Godvin Sharmila, V. Combination of Electrocoagulation with Solar Photo Fenton Process for Treatment of Landfill Leachate. *Environ. Technol.* **2023**, *44*, 4441–4459. [CrossRef]